On Serrated Plastic Flow in an AA5052-H32 Sheet

Wei Tong[1]
e-mail: wtong@smu.edu

Nian Zhang

Department of Mechanical Engineering,
Yale University,
New Haven, CT 06520-8284

Temporal and spatial characteristics of serrated plastic flow or the so-called Portevin-Le Chatelier (PLC) deformation bands in a commercial Al-2.5%Mg *sheet metal due to dynamic strain aging effects were investigated experimentally under quasi-static uniaxial tension. It was found that the thickness and width of test coupons, applied loading conditions (machine stiffness and crosshead speed), and mechanical polishing had an observable effect on the temporal characteristics of the serrated plastic flow while short and long interruptions during the tensile tests with stress relaxation and even completely unloading show minimal effects on the subsequent serrated flow behavior. Serrations in axial load in AA5052-H32 were found to associate with the appearance of discrete narrow deformation bands in the tensile test coupons with the bands aligned* 59 ± 1 deg *with respect to the tensile loading axis. The detailed strain distribution across the deformation bands showed a bell-like instead of steplike shape, indicating that the formation of these deformation bands was controlled by a local nucleation and growth process at a cross section in the polycrystalline sheet.* [DOI: 10.1115/1.2712466]

1 Introduction

Plastic flow in metals and alloys at ambient condition is originated from generation and motion of dislocations through their crystallographic lattices [1]. The deformation process at the microscopic level is temporarily discontinuous and spatially discrete, but the overall behavior of a polycrystalline metal is often shown to have a stable flow stress strain curve and a smooth plastic flow pattern at the macroscopic level. However, macroscopic unstable plastic flow in terms of serrated yielding and deformation bands can also be manifested in metals and alloys exhibiting strong static and dynamic strain aging effects [1–4]. One of the clearest examples of the so-called Portevin-Le Chatetlier or dynamic strain aging effect is the plastic flow behavior of dilute Al-Mg alloys under uniaxial tension [3,4]. Although the unstable plastic flow behavior in these metals is generally understood as the consequence of solute-dislocation interaction at the microscopic level as proposed by Cottrell [1] over a half century ago, a complete understanding on detailed micromechanical mechanisms and various factors that may affect the macroscopic behavior of serrated plastic flow remains lacking. Besides that the PLC effect involves collective behavior of large dislocations in a complex manner, the exact nature of the serrated plastic flow has rarely been characterized in details even at the macroscopic level.

Here, we present an experimental study on characterizing, both temporally and spatially, the serrated plastic flow in an Al-Mg alloy (AA5052-H32). As computer-assisted analyses of serrations in the time domain have now been widely used to evaluate the PLC effect in a material [5–7], one of the major objectives in our study is to evaluate to what a degree that various factors (size and geometry of test coupons, test machines, mechanical polishing, and loading interruptions) may affect the temporal characteristics of serrated flow in AA5052-H32. Another objective of our study is to measure the morphology of individual PLC bands in terms of detailed strain distributions by digital image correlation [8–12] to shed some light on the possible mechanism and process when each band is generated. In the following, the material and experimental procedure used in our study are described first in Sec. 2. The experimental results are then presented in Sec. 3 in terms of temporal and spatial characteristics of serrated plastic flow. Discussion is given in Sec. 4 on the morphology of PLC bands, the sensitivity of serrations on various factors, the effect of anisotropic plasticity on the band orientation angle, and the unique advantage of the high-resolution digital imaging and the associated correlation-based strain-mapping technique for studying the spatial morphology of PLC bands. Conclusions of our study are summarized in Sec. 5.

2 Experimental Procedure

The material studied in this investigation was a commercial aluminum-magnesium alloy AA5052-H32 sheet with major alloying elements of 2.5 wt. % Mg and 0.25 wt. % Cr [13]. The as-received polycrystalline sheet had the strain-hardened and stabilized H32 temper and was not strongly textured. It had a thickness of 0.95 mm and an average grain size of $\sim 12\ \mu$m. Two types of uniaxial tensile test coupons were machined from the AA5052-H32 sheet, with their axial loading directions aligned with the sheet rolling direction. The first type, designated as a standard test coupon (ST), had a gauge section with dimensions of 12.65 mm wide and 67 mm long, similar to the standard ASTM E8 flat metallic tension coupons. The second type, designated as a compact test coupon (CT), had a size of about 1/3 of the standard ones (with a gage section of 4.6 mm wide and 20 mm long). As shown in Table 1, a total of five compact test coupons (CT1–CT5) and two standard test coupons (ST#1 and ST#2) were tested in this study. Four of the five compact test coupons had a reduced thickness ranging from 0.21 mm to 0.93 mm by means of mechanical grinding and polishing using metallurgical papers. One polished test coupon (CT1) was also slightly etched in a solution of 40 ml H_3PO_4, 5 ml HNO_4, and 5 ml H_2O at $\sim 100\,^{\circ}$C for 20 min and was used for microtexture measurements by electronic backscattered diffraction pattern analysis. All of other three test coupons (CT3, ST1, and ST2) had the original sheet thickness of 0.95 mm and were tested in the as-received condition.

The standard test coupons were loaded on a hydraulic material testing system (MTS model 810) with a 20 kN load cell while the compact test coupons were stretched by a screw-driven mini-tensile tester (100 mm $\times$ 125 mm $\times$ 50 mm in total dimensions, a total crosshead travel of 50 mm, and a load cell of 4.4 kN maximum capacity). During the testing of the two compact test coupons CT1 and CT5, two long interruptions ($\sim$2 h each interruption) and multiple short interruptions (100–140 s) were imposed, respectively. In each test, the thin flat test coupon was fully clamped at both ends and stretched under displacement control at

[1]Corresponding author.

Contributed by the Materials Division of ASME for publication in the JOURNAL OF ENGINEERING MATERIALS AND TECHNOLOGY. Manuscript received May 24, 2004; final manuscript received September 1, 2006. Review conducted by Hamid Garmestani.

Table 1 Summary of Uniaxial Tensile Tests of AA5052-H32 Sheets

Sample No.	CT1	CT2	CT3	CT4	CT5[a]	ST1	ST2[b]
Thickness h_0 (mm)	0.91	0.93	0.95	0.21	0.93	0.95	0.95
Width w_0 (mm)	4.55	4.60	4. 60	4.56	4.62	12.65	12.65
Gage section length L_0 (mm)	20.0	20.0	20.0	20.0	20.0	67.0	67.0
Cross-sectional area A_0 (mm^2)	4.16	4.32	4.32	0.91	4.33	11.8	11.8
Crosshead speed V (μm/s)	0.6	1.0	1.0	1.0	1.0	2.0	10.0
Nominal strain rate $\dot{\varepsilon}$ (1/s)	3×10^{-5}	5×10^{-5}	5×10^{-5}	5×10^{-5}	5×10^{-5}	3×10^{-5}	1.5×10^{-4}
Effective stiffness M (MN/m)	5.8	5.1	3.8	1.3	3.5	6.9	6.5
Effective modulus $\bar{E}$(GPa)(***)	71.5	57	43.5	70	44.5	8.8	8.2
Typical serration periods Δt (s)	7.1	7.8	7.7	2.9	8.6	9.6	2.3
Typical load drop ΔP (N)	25	32	29	4.2	28	97	80
Typical stress drop $\Delta\sigma$ (MPa)	6.1	7.4	6.7	4.6	6.5	8.2	6.8
Reloading rate $\dot{P}_r$ (N/s)	3.5	4.1	3.7	1.45	3.3	10.1	34.8
Reloading stress Rate $\dot{\sigma}_r$ (MPa/s)	0.86	0.95	0.86	1.59	0.76	0.85	3.0
Typical normalized serrations $\Delta P/P$ (%)	2.6	3.0	2.8	2.2	2.9	3.4	2.7

[a]Interrupted tensile test with digital images acquired (1 pixel=9.9 μm).
[b]Continuous tensile test with digital images acquired (1 pixel=37.4 μm).
[c]Assuming that only the tensile test coupon deformed during the reloading step.

a constant crosshead speed to achieve a range of nominal strain rates from 3×10^{-5} 1/s to 1.5×10^{-4} 1/s. Both force and displacement data in the majority of the tests were recorded digitally at a rate of 8 Hz. A data acquisition rate of 100 Hz was used occasionally in some selected tests as well. The uncertainty in the load measurement was ±7 N and ±0.3 N for the 20 kN and 4.4 kN load cells, respectively.

To characterize the PLC bands spatially, the entire gage sections of one standard test coupon (ST2) and one compact test coupon (CT5) were imaged during tensile testing. Prior to the test, one flat surface of each tensile test coupon was decorated with finely sprayed black paint speckles to enhance the image contrast. The standard tensile coupon ST2 was imaged periodically at an interval of 4–20 s using a digital camera (Canon EOS Digital Rebel). Each of the recorded digital images had a size of 3072 $\times$2048 pixels with a spatial resolution of 37.4 μm per pixel. The standard test coupon ST2 was stretched continuously by the MTS 810 testing machine to failure without any pausing while digital images (24-bit color) were recorded at a shutter speed of 1/100 s. On the other hand, tensile testing of the compact test coupon CT5 was interrupted frequently by completely stopping the step motor of the mini tensile tester after either a single serration or a series of serrations occurred. The compact test coupon CT5 was then imaged using a monochromic charge-coupled device (CCD) video camera with a telecentric zoom lens (55 mm/F2.8, Edmund Scientific Co.). A frame grabber board (Data Translation DT3152) was used to digitalize the video frame into eight-bit gray-scale digital images with a size of 640$\times$480 pixels and a spatial resolution of 9.9 μm per pixel. To reducing image noises, each digital image was acquired by averaging a total of 60 video frames while the step motor of the mini tensile tester remained stopped. The CCD video camera was mounted on a XYZ translation stage and a series of four to five digital images were recorded by moving the CCD video camera along the axial loading direction to cover the entire gage section. A typical assembled image from these slightly overlapped digital images had a size of 2250$\times$480 pixels. The recorded digital images were analyzed by an image correlation surface deformation mapping software developed in our own laboratory to obtain both cumulative and incremental surface strain maps of the test coupons. Details on the strain mapping via the image correlation analysis have been given elsewhere [8–12]. The errors in local in-plane displacements, rigid-body rotation, and strain measurements were estimated to be about 0.02 pixels, 0.02 deg, and 400×10^{-6}, respectively, for a macroscopically homogenous field [10].

3 Experimental Results

Table 1 presents a brief summary on the sample dimensions and loading conditions used in the seven uniaxial tension tests on AA5052-H32 (the machine stiffness (M) was computed based on the reloading slopes after load drops). Serrated plastic flow occurred in all of seven tests at the ambient condition according to the recorded axial load versus time data. Plastic deformation maps of the tensile test coupons in two tensile tests (CT5 and ST2) have also been obtained by image correlation analysis. Both temporal and spatial characteristics of the serrated plastic flow in AA5052-H32 observed in these tests are presented in the following.

3.1 Temporal Characteristics of Serrated Plastic Flow. The load P versus time t data for the test coupons CT2 and ST1 are shown in Figs. 1(a) and 2(a), respectively. Although the nominal applied strain rates in both tests were comparable (5×10^{-5} 1/s and 3×10^{-5} 1/s), serrations in axial load occurred immediately after the plastic yielding in test coupon CT2 (mechanically polished) but commenced until after ~1% plastic strain in test coupon ST1 (as-received). An expanded view of the selected successive load serrations at a later stage of each test is shown by the insert in both Figs. 1(a) and 2(a). The incubation

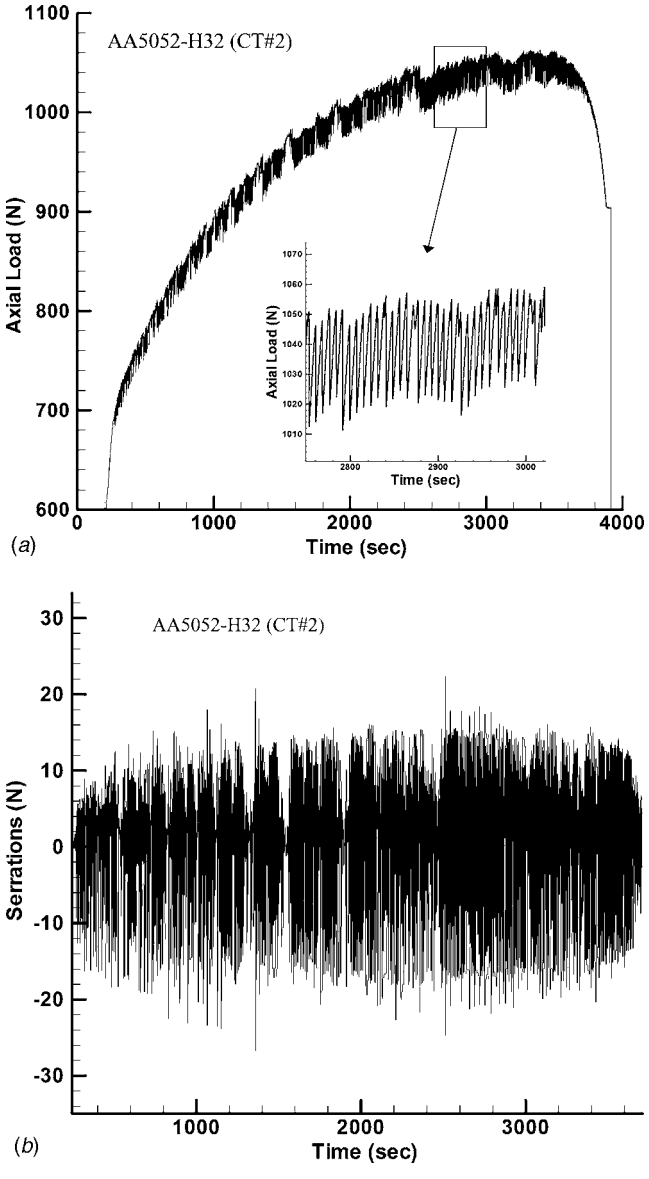

Fig. 1 Uniaxial tensile serrated flow curves of AA5052-H32 compact test coupon CT2 (surface condition: mechanically polished): (*a*) originally recorded axial load versus time data and (*b*) serrations in terms of deviations ΔP from the average axial load $\bar{P}$

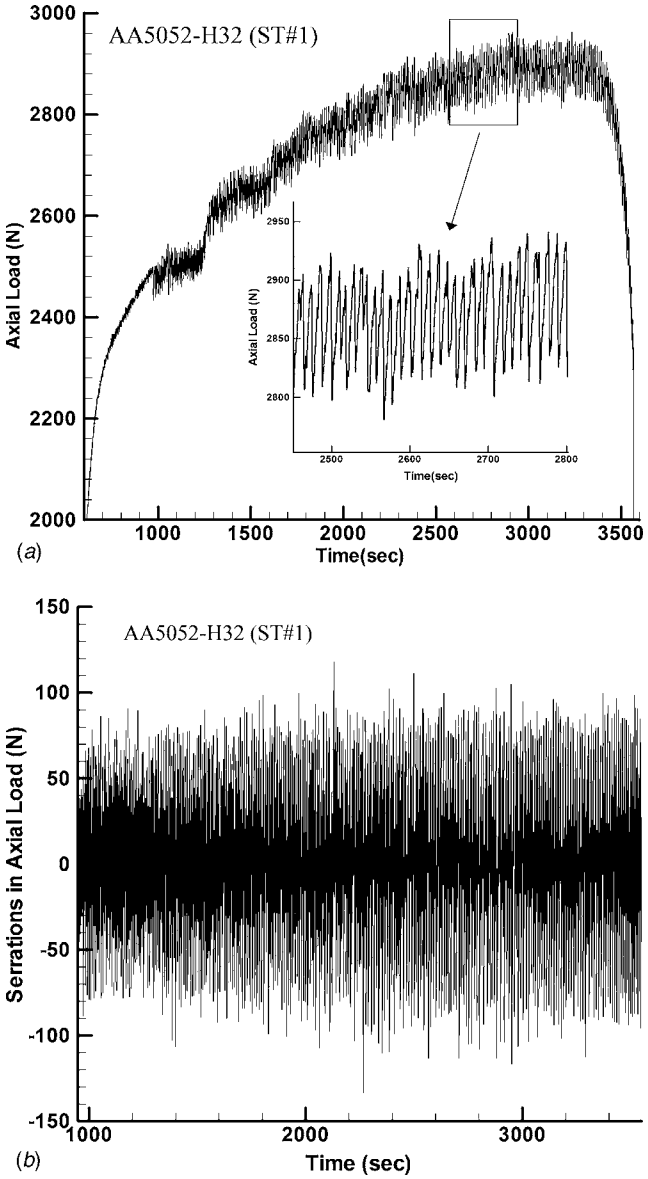

Fig. 2 Uniaxial tensile serrated flow curves of AA5052-H32 standard test coupon ST1 (surface condition: as-received): (*a*) originally recorded axial load versus time data $P(t)$; and (*b*) serrations in terms of deviations ΔP from the average axial load $\bar{P}$

strain of ~1% was also observed in the compact test coupon CT3 (as-received). As the AA5052-H32 sheet exhibits a significant degree of strain hardening initially, the magnitude of load serrations over the time in a test can be better illustrated by using the deviation in axial load (ΔP) (see Figs. 1(*b*) and 2(*b*)). The deviation in axial load was computed by subtracting the average axial load ($\bar{P}$) from the recorded axial load: $\Delta P = P - \bar{P}$. The average axial load was obtained by smoothing out all high-frequency variations in the original axial load data. The magnitude of the serrations in load was found to be around 30 N and 100 N for tests CT2 and ST1, respectively, and it increased slightly with increasing plastic deformation. The entire serrated flow data of four tensile tests (CT2, CT4, ST1, and ST2) are summarized in Fig. 3(*a*) in terms of the normalized serrations $\Delta P/\bar{P}$ to account for the increased flow stress due to strain hardening and the difference in the cross-sectional areas among test coupons. A more detailed view of about 40 individual serrations in terms of flow stress $\Delta\sigma = \Delta P/A_0$ (where A_0 is the initial cross-sectional area of a test coupon) is given in Fig. 3(*b*). Those 40 or so serrations occurred at a later stage in each of the four tensile tests when the strain hardening effect was significantly diminished (see Figs. 1(*a*) and 2(*a*)).

Hundreds of serrations were detected in each tensile test up to a plastic strain of 10% or higher and each serration event consisted of a sudden load drop in ~0.03 s or less and a relatively much slower reloading step in a duration of 2–10 s or more, depending on the applied crosshead speed and testing machine used in a tensile test (see Table 1). The magnitude of serrations in flow stress varied mostly between about 2% and 4% of the current flow stress level of the material (Fig. 3(*a*)). A thinner test coupon (CT4) showed smaller but faster serrations than a thicker test coupon (CT2). On the other hand, a wider test coupon (ST1) showed only slightly larger but slower serrations (as compared to test coupon CT1; see Table 1). That is, the reduction in test coupon thickness had a much significant effect on the serrations (in both magnitude

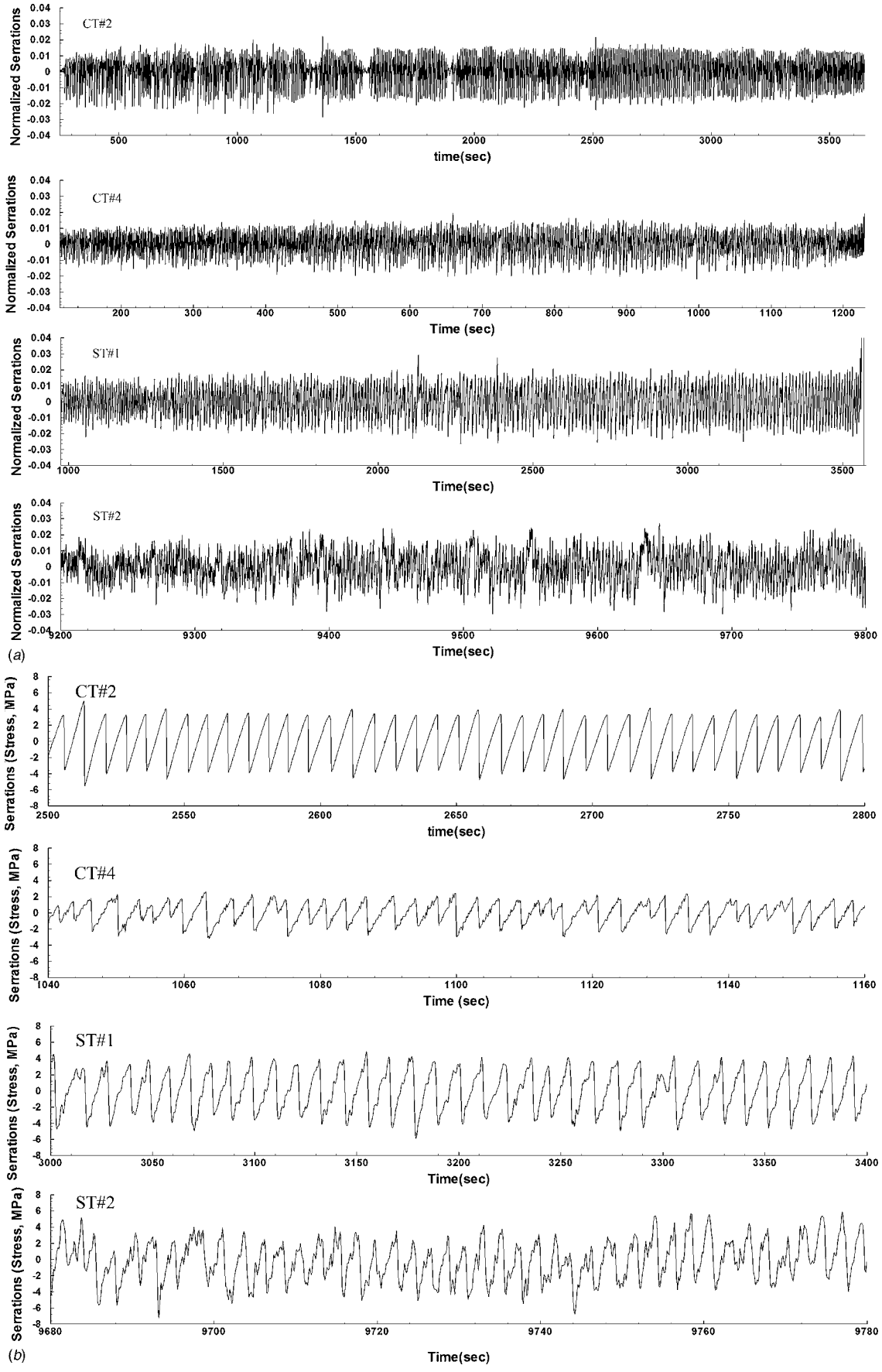

Fig. 3 Comparison of serrated flow curves of four test coupons (CT2, CT4, ST1, and ST2): (*a*) the normalized serrations $\Delta P/\bar{P}$ and (*b*) an expanded view of selected serrations in flow stress $\Delta\sigma=\Delta P/A_0$

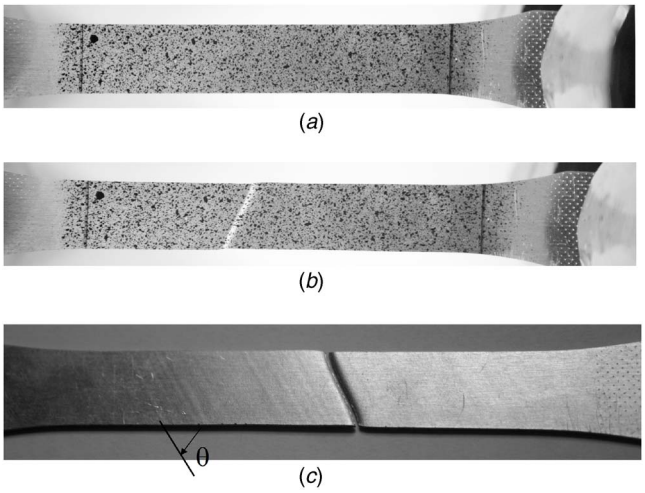

Fig. 4 Images of test coupon ST2: (*a*) the initially undeformed coupon, (*b*) appearance of a diffuse neck prior to final failure, and (*c*) surface markings due to PLC bands (after fracture). Images (*a*) and (*b*) are the front surface decorated with sprayed black paint speckles, and image (*c*) is the back surface without paint speckles illuminated at a glancing angle. The orientation angle (θ) of the PLC bands was about −59 deg (clockwise).

and period). For a given test coupon geometry and the same testing machine, the increase in the applied nominal strain rate induced faster and slightly smaller serrations as well (see ST1 versus ST2 in Table 1). When the serration period (the time interval between serrations) was 7–10 s or longer, the serrations had a more or less uniform magnitude (see CT2 and ST1 in Fig. 3(*b*)). Serrations with short periods (say, 2–3 s) showed a much large scattering in their magnitude (see CT4 and ST2 in Fig. 3(*b*)).

3.2 Spatial Characteristics of the PLC Bands in the Standard Test Coupon ST2. As described in Sec. 2, the test coupon ST2 was stretched continuously and one of its flat surfaces was imaged periodically by a digital camera at a shutter speed of 1/100 s. Figures 4(*a*) and 4(*b*) show the two of the 128 acquired digital images of test coupon ST2 (the initially undeformed and the localized necking just prior to final failure). The front surface of the gage section was decorated with sprayed black paint speckles, and two black marked lines indicates approximately the end of the gradually tapered shoulder sections and the beginning of the straight gage section. Also shown in Fig. 4(*c*) is the back surface of the test coupon imaged after fracture. Markings of a series of parallel PLC bands oriented in an angle of $\theta \approx -59$ deg (clockwise) with the tensile axis are faintly visible on the surface that was not sprayed with black paint speckles. The spatial characteristics in terms of plastic strain patterns of the individual PLC bands in AA5052-H32 are illustrated in Fig. 5(*a*) by a set of eight successive incremental plastic strain maps. The eight incremental plastic strain maps were obtained by a correlation analysis of adjacent image pairs of nine images (Nos. 718–726) recorded during the experiment, and they reflected the active plastic flow events occurred within the time interval of 4–6 s when a pair of images was taken. Figure 5(*b*) shows the corresponding temporal characteristics in terms of load drops of the PLC bands captured in the eight incremental strain maps. The number of PLC bands in a strain map based on an image pair shown in Fig. 5(*a*) was found to be identical to the number of major sudden load drops shown in Fig. 5(*b*) between the time interval when the image pair were recorded. A grid point spacing of 5×5 pixels and a subset size of 30×30 pixels were used in the image correlation analysis (noting each pixel corresponds to 37.4 μm in these digital images). Also shown in Fig. 5 are the corresponding eight digital images of the test coupon. Each of these digital images was obtained by subtracting a digital image from its adjacent one and followed by an equalization adjustment of its histogram so the change of the optical intensity on the test coupon surface was magnified. Bandlike surface markings (with a number from one to four) can be seen in these enhanced digital images in Fig. 5, and these markings were confirmed by the corresponding incremental plastic strain maps to be deformation bands with a significantly higher axial strain inside them. The deformation bands are of the so-called type-C Porvetin Le-Chatelier bands that were distinctly discrete and nucleated more or less randomly along the gauge section of the test coupon. Some of the PLC bands appeared in the tapered shoulder sections of the test coupon as well (see the No. 1 and No. 5 images and maps in Fig. 5). The strain mapping results were less accurate in the shoulder section due to lack of optical contrast in the digital images (as no black paint speckles were applied to the shoulder sections; see Fig. 4(*a*). For a given time interval when a pair of digital images was taken, the number of serrations detected in the time versus load data was found to be identical to the number of individual bands detected by the digital images. The PLC bands shown in Fig. 5 are all tilted to the right with an angle of 59±1 deg (counterclockwise) with respect to the horizontal tensile loading axis of the test coupon. In the early and later stages of the plastic deformation of test coupon ST2, a few PLC bands tilted to the left with an angle of 59±1 deg were also occasionally detected.

Figure 6 shows the distribution of axial normal strain along the centerline of the gage section of test coupon ST2 for the selected eight image pairs shown in Fig. 5. The peak strain inside each deformation band varies from 0.6% to 1.5%, and the band width measured in terms of the full width at half height (FWHH) of each strain distribution profile is between 1.5 mm and 2.5 mm. As a comparison, the surface markings in digital images shown in Fig. 5 have a width of about 30 to 40 pixels (i.e., 1.1–1.5 mm).

3.3 Spatial Characteristics of the PLC Bands in the Compact Test Coupon CT5. The testing of compact test coupon CT5 was interrupted periodically by stopping the step motor of the mini tensile tester for 100–140 s, and multiple digital images were taken to cover the entire gage section at each interruption. One unique aspect of this test was that the testing was interrupted after single as well as multiple serrations were observed. Figure 7 shows the load versus time data for the test, which consisted of 20 loading steps with only a single serration and 20 loading steps with multiple serrations. Image pairs were analyzed for each loading step with only a single serration. A grid point spacing of 5 $\times$5 pixels and a subset size of 50×50 pixels were used in the image correlation analysis (noting the digital images acquired in this test had a spatial resolution of 9.9 μm per pixel). Half of the 20 loading steps with a single serration produced a single PLC band well within the gage section of the test coupon, while other half of the loading steps produced a single PLC band in the shoulder and gripping sections of the test coupon. The spatial morphology of these ten PLC bands within the gage section is shown in Fig. 8. These PLC bands shown in Fig. 8 are tilted alternatively both to the left and to the right with an angle of 59±1 deg with respect to the horizontal tensile loading axis of the test coupon. Figure 9 shows the distribution of axial normal strain along the centerline of the gage section of test coupon CT5 for the ten PLC bands shown in Fig. 8. The peak strain inside each deformation band varied from 0.44% to 1%, and the bandwidth measured in terms of the full width at half height (FWHH) of each strain distribution profile was between 0.75 mm and 1.75 mm.

4 Discussion

Unstable plastic flow in metals and alloys under uniaxial tension have often been classified into two major categories [2,4]: (i) The Lüders band that is associated with normally a single set of upper and lower yield points and (ii) the Portevin-Le Chatelier band that is associated with repeated serrations as observed in the

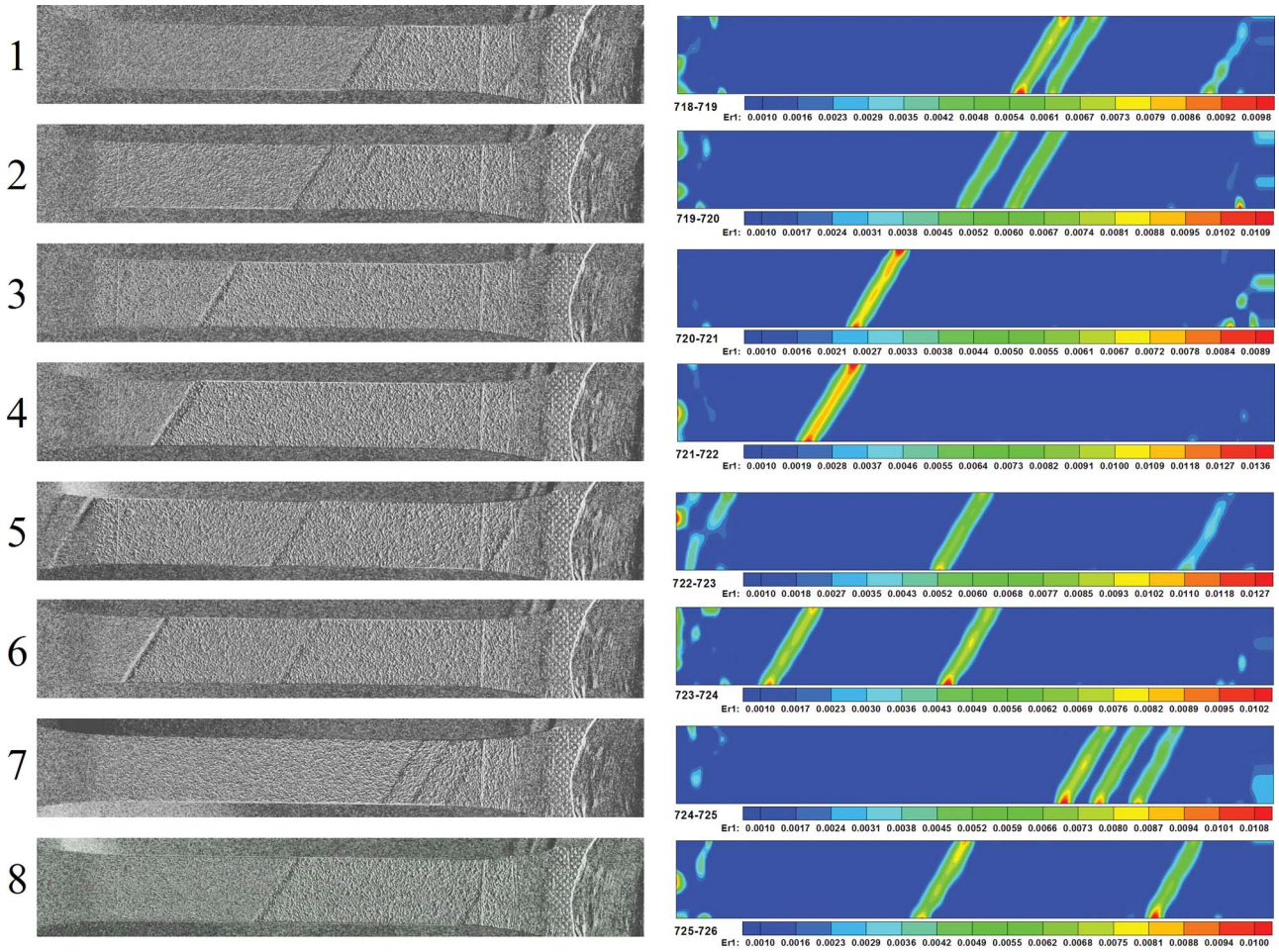

(*a*)

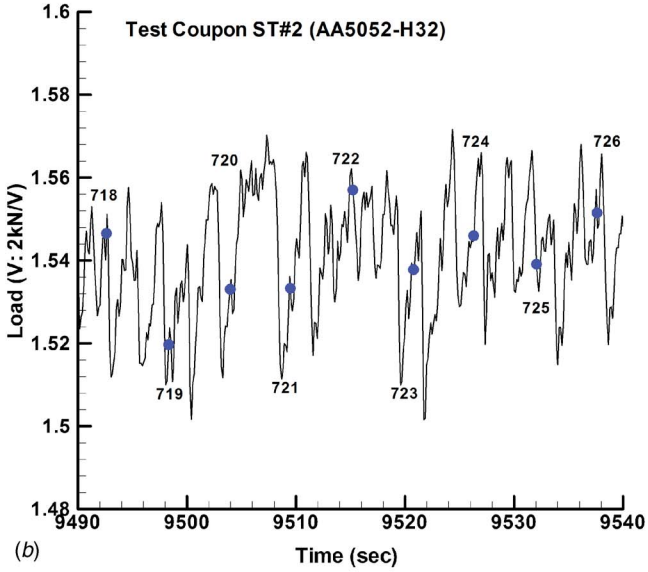

(*b*)

Fig. 5 (*a*) **Spatial morphology of PLC bands in test coupon ST2 captured by nine consecutive images Nos. 718–726. The eight images on the left show the enhanced differential optical contrast due to PLC bands while the eight axial strain contour maps show the incremental strains accumulated during the time interval of recording each adjacent image pair.** (*b*) **The corresponding temporal characteristics in terms of a sudden load drop per PLC band for the interval of each image pair. The numbers 718–726 designate the image frames and the corresponding filled circles mark the times and load levels at which the nine image frames were recorded in the experiment.**

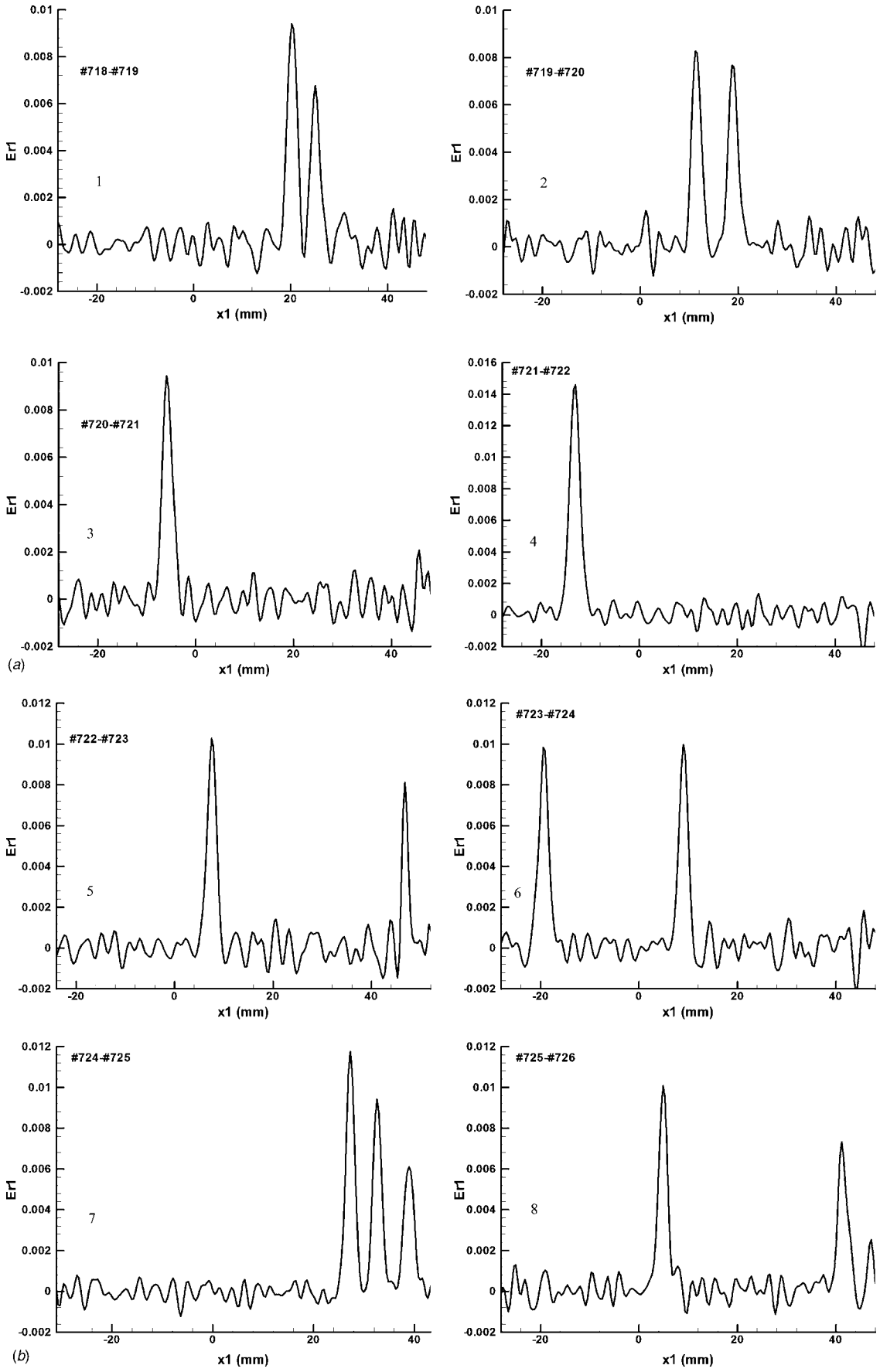

Fig. 6 Axial strain distribution profiles 1–4 (*a*) and 5–8 (*b*) along the tensile axis of test coupon ST2. The eight axial strain (Er1) distribution profiles are extracted from the horizontal centerline (x1) in each of the eight incremental strain maps shown in Fig. 5.

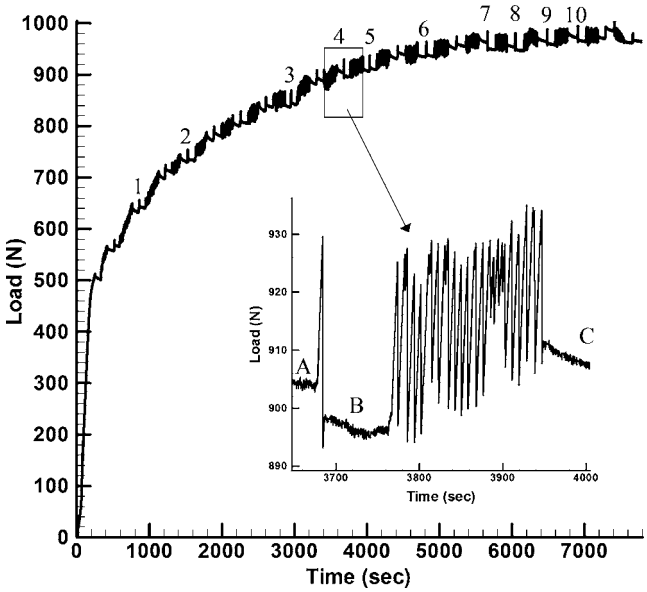

Fig. 7 Uniaxial tensile serrated flow curve of AA5052-H32 compact test coupon CT5. The repeated relaxation in axial load (e.g., see points A, B, and C in the insert) is due to the imposed multiple complete stops of the step motor of the mini tensile tester. The numbers on the curve designate the ten single serrations that occurred within the gauge section and were captured by digital images.

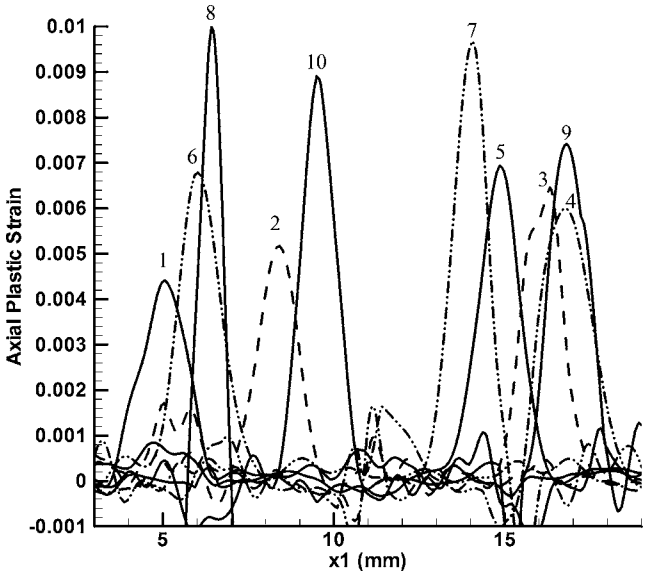

Fig. 9 Axial strain distribution profiles along the tensile axis of test coupon CT5. The ten strain distribution profiles are extracted from the horizontal centerline in each of the ten incremental strain maps shown in Fig. 8.

AA5052-H32 sheet in this study. Upon the load drop from the upper yield point to the lower yield point, a Lüders band usually nucleates at one shoulder end of the test coupon and propagates continuously toward the other end at the constant lower yield point flow stress level. Once the test coupon is uniformly deformed at the so-called Lüders strain throughout the gage section, the plastic deformation proceeds stably and uniformly at the macroscopic scale with positive strain hardening. On the other hand, the PLC band (type C) nucleates and grows more or less randomly or spatially uncorrelated all over the test coupon in a very short duration of each load drop [4,14–24]. Contrary to the commonly held assumptions that type C PLC bands may have well-defined sharp front and rear edges during its growth stage and a final uniform strain distribution [4], our detailed plastic incremental surface strain mapping results of both test coupons CT5 and ST2 show instead that each PLC band has a bell-like strain distribution with a peak strain right in the center of the band and a gradual reduction in strain at the band edges. In particular, the results of test coupon CT5 unambiguously indicated that there are no step-like strain distributions at the PLC band edges as the strain maps of the ten single PLC bands associated with ten single serrations in test coupon CT5 have an exceedingly high spatial resolution of 49.5 μm per grid point (recall that the grid point spacing of five pixels in the image correlation analysis and the pixel resolution of 9.9 μm). Consequently, the plastic deformation accumulated inside a PLC band under constant crosshead speed loading is most likely due to a burst of the high strain-rate event of *spontaneous* nucleation, growth, and decay, and it is not due to the propagation of a sharp deformation front from one edge to another edge of the PLC band in the axial loading direction during each load drop. Newly obtained experimental results based on time-resolved strain mapping measurements using an ultrahigh-speed digital camera are found to be consistent with these observations [19].

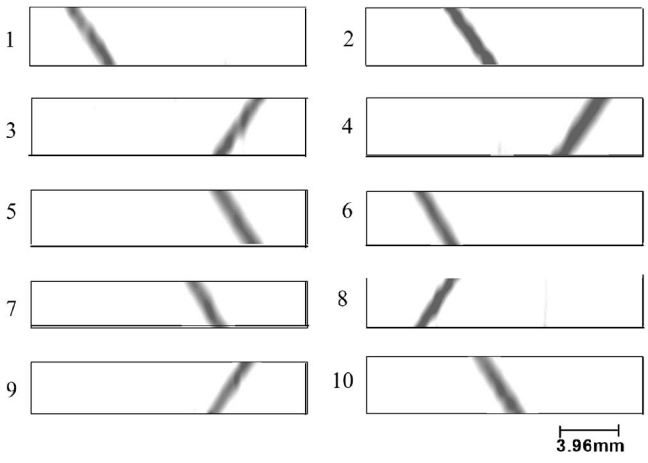

Fig. 8 Spatial morphology of ten PLC bands (in gray scale) in test coupon CT5. The ten PLC bands correspond to the ten single serrations in axial load shown in Fig. 7. A threshold of 0.2% axial strain was used in generating the gray-scale contour of axial strain distribution in each strain map.

Our experimental results have shown that interruptions longer than 100 s in a tensile test of AA5052-H32 test coupons did not significantly affect the subsequent serrated plastic flow behavior. The tensile test of test coupon CT1 was interrupted to complete unloading for 2 h at 5% and 10% plastic strain, respectively. The tensile test of test coupon CT5 was interrupted periodically for stress relaxation of 100–140 s after either single or multiple serrations. The resulting serrations in CT1 and CT5 were found to be similar to those found in test coupon CT2 (continuous tensile loading). It appears that dynamic strain aging occurred and completed in a fairly short duration (tens of seconds at most), and there was little additional static strain aging effect at all in AA5052-H32. On the other hand, our experimental results have shown that the temporal characteristics of serrated plastic flow are rather sensitive to the geometry or size of test coupons (especially the coupon thickness), loading machine stiffness, and even mechanical polishing. For example, using the same mini tensile tester and under the identical constant crosshead speed loading, normalized serrations in a thinner test coupon (CT4) were much faster and lower in magnitude that those in a thicker test coupon (CT2) (see Fig. 3(*b*)). Normalized serrations of a wider and longer test coupon (ST1) were somewhat slower and higher in magnitude (cf.

CT1), although both tests were carried out at the same overall strain rate and reloading stress rate (see Table 1). Consequently, any simple statistical analysis of serrations in the time domain [5–7] should be treated with caution, because there exists a strong coupling between the intrinsic material constitutive behavior and external mechanical boundary conditions [15–23]. Comparison between different tensile tests even under the same nominal strain rate may not be meaningful if the effects of geometry and size of test coupons and boundary loading conditions (such as machine stiffness) imposed by different test machines were not considered as well (e.g., by means of two-dimensional (2D) or even three-dimensional (3D) finite element full field analyses). As a PLC band was developed during each load drop in a very short time interval of 0.03 s or less, the actual local strain rate inside the band could be at least as high as 0.1–1.0 1/s or more (recalling the peak band strain varied from 0.4% to 1.5%).

The existence of an incubation or critical strain for serrated plastic flow has been attributed to the requirement of PLC effects on the solute atom mobility that can be enhanced by the increasing bulk vacancies due to plastic deformation [4,18]. It is interesting to note that the onset of serrated plastic flow in thin sheets can be advanced right to the start of plastic yielding by using much thinner test coupons. One possible explanation is that plastic deformation in the thin surface layer of the AA5052-H32 sheets through the normal metallurgical polishing (for preparation of thinner coupons) was sufficient to promote their solute atom mobility. Another plausible explanation is the stronger free-surface effect (via the stronger image force acting on the dislocations inside the sheet metal) in thinner coupons. As our experimental results show that type C PLC bands grow and decay *spontaneously* in a localized and nonpropagating manner, the occurrence of type-C PLC bands is a nucleation-dominant event. Thus, the existence of nucleation centers or sites and the stress level that exceeds the critical band nucleation threshold (through at least the thickness of a thin sheet) are the necessary and sufficient conditions, respectively. The so-called incubation or critical strain for the serrated plastic flow of type C can then be understood as the need to raise the stress level (via strain hardening) in the test coupon up to the band nucleation threshold. The disappearance of the incubation strain in the thinner and or polished test coupons can be understood as the reduction of the threshold stress level for band nucleation. Furthermore, the difference between the type-B (spatially correlated) and type-C (spatially uncorrelated) PLC bands can be understood as the difference of the material heterogeneity in terms of the band nucleation threshold: type-B bands occur when the material is rather homogenous and the slight stress increase due to a band formation is sufficient to exceed the nucleation threshold of the neighboring material. On the other hand, type-C bands appear when the material is highly heterogeneous in terms of the band nucleation conditions. Clearly, further systematic research on the *band nucleation conditions* in terms of material processing and sample preparation as well as the underlying dislocation dynamics at the meso scale of the sheet thickness is of great importance. Existing theoretical modeling efforts [16,17,20–24] thus far have mostly focused on the behavior of type-A (continuously propagating) PLC bands and have not successfully and satisfactorily addressed this critical issue related to the understanding of the nonpropagating type-B and type-C PLC bands.

Although the formation of PLC bands occurred locally in a narrow cross-sectional region of a test coupon in a very short time due to the release of aged dislocations in the material, these deformation bands should nevertheless still obey the macroscopic kinematics constraints on the plastic flow. The later can be illustrated by considering the orientation of PLC bands. Based on the plastic strain mapping results for ST2 and CT5, the ratio of the transverse over the axial plastic strain α was found to be -0.38 (so the plastic strain ratio R of the AA5052-H32 sheet is 0.61). If a PLC band was indeed treated as a localized neck oriented toward the line of zero extension as suggested by Hill [25] in the flat surface of the test coupon, then one has (based on the coordinate transformation of strain tensor and our experimental data showing that the shear strain increment $\Delta\varepsilon_{12}$ was negligible in uniaxial tensile tests)

$$\Delta\varepsilon_1^b = \frac{\Delta\varepsilon_1 + \Delta\varepsilon_2}{2} + \frac{\Delta\varepsilon_1 - \Delta\varepsilon_2}{2}\cos 2\theta = 0 \tag{1}$$

or

$$\cos 2\theta = -\frac{1+\alpha}{1-\alpha} \tag{2}$$

where $\Delta\varepsilon_1^b$ is the strain increment along the direction of a PLC band, $\Delta\varepsilon_1$ and $\Delta\varepsilon_2$ are the strain increments in the axial and transverse directions of the test coupon in the PLC band, and θ is the angle between the PLC band and the axial loading direction (see Fig. 4(*c*)). Using the measured $\alpha=-0.38$, one obtains $\theta = \pm 58.3$ deg, which are virtually identical to the PLC band orientation angles $\pm 59 \pm 1$ deg measured for both test coupons CT5 and ST2. The PLC band orientation angle is different from ± 54.7 deg (for an isotropic material with $\alpha=-0.5$) reflects the fact that the plastic flow inside a PLC band is still affected by the macroscopic anisotropy of the polycrystalline material. The explanation on the inclined PLC bands based on the microscopic mechanism of collective dislocation motion over multiple grain boundaries given by Wen and Morris [18] is thus questionable as the plastic strain ratio R is known to be related to the texture of the polycrystalline metals, and there is no direct experimental evidence supporting either the collective motion of dislocations or the propagation of type-B or type-C PLC bands in the axial loading direction.

The machine equation for the uniaxial tensile test under displacement control can be written as [16,17]

$$V_0 = \frac{\dot{F}}{K} + \int_0^L \dot{\varepsilon}_1^p(x_1,t)dx_1 \tag{3}$$

where V_0 is the imposed constant crosshead speed at the ends, K is the total axial stiffness of the machine and the specimen, $\dot{F}$ is the axial loading rate, L is the entire length of the tensile sample between the grips, and $\dot{\varepsilon}_1^p$ is the axial plastic strain rate along the loading direction. When a type-C PLC band nucleates and grows over a short period of time Δt, one can integrate Eq. (3) to obtain

$$V_0\Delta t = -\frac{\Delta F}{K} + \int_0^{w_b} \Delta\varepsilon_{b1}^p(x_1,t)dx_1 \tag{4}$$

where ΔF is the magnitude in a sudden load drop corresponding to the PLC band creation, and $\Delta\varepsilon_{b1}^p$ is the axial plastic strain increment accumulated only inside the band with a width w_b. When the strain profile inside a band is approximated as a triangular shape and the PLC band develops quickly (i.e., Δt is sufficiently small so $V_0\Delta t$ is negligible), one has

$$\Delta F \approx K w_b^h \Delta\varepsilon_b^{\max} \tag{5}$$

where $\Delta\varepsilon_b^{\max}$ is the maximum or peak strain *increment* inside a PLC band and w_b^h is the FWHH measured from an incremental axial strain profile of the PLC band (e.g., see Figs. 6 and 9). Indeed, this investigation shows that a simple relationship between the magnitude of peak strain inside a PLC band and the magnitude of load drop in each serration did not exist as the width of a PLC band was not constant at all for the same tensile specimen. Consequently, the common use of the magnitude of stress drop in either experimental data analysis [18,21] or theoretical modeling [21,22] may not be valid without additional information on the sample thickness and machine stiffness as well as the more detailed measurements on the band strain $\Delta\varepsilon_b^{\max}$ and band width w_b^h.

Direct visual inspection and video imaging of a smooth or polished surface illuminated at a glancing angle has been traditionally used to characterize the spatial morphology of PLC bands based on the optical contrast induced by local surface roughening [2,14]. As the optical contrast is often diffuse, the use of such a method to measure the width of a band may depend on the illumination conditions. Once the virgin surface of a test coupon is covered with the first set of PLC bands, it becomes increasingly difficult to discern additional PLC bands over the plastically deformed rough surface. The direct optical contrast method cannot provide any quantitative information on the strain distribution as well. Similarly, the laser scanning extensometry technique recently used by Hahner et al. [20] and Klose et al. [21,22] limits only to the one-dimensional (longitudinal or axial strain) measurement of insufficient spatial resolution and strain sensitivity. The technique of high-quality digital imaging of a test coupon surface decorated with sprayed paint speckles presented in this study is much superior in characterizing PLC bands. Besides, the digital images can be used via a float-point correlation analysis to obtain detailed *incremental* plastic strain mapping data of the PLC bands, the *differential* optical contrast among these digital images can also be extracted and enhanced following the procedure described in this study to be used to visualize individual PLC bands through out the entire deformation process (see Fig. 5). Surface preparation by mechanical polishing is unnecessary (which may also affect the serrated plastic flow behavior in thin sheets as it may alter the band nucleation threshold) as the new technique is applicable to both smooth and roughened surfaces. However, digital images with large-format sizes are needed to achieve a sufficiently high spatial resolution for both visualization and strain mapping analysis of PLC bands. Digital video and other high-speed digital imaging systems (with somewhat reduced image format sizes) may be used to increase the time resolution so even the type-A (continuously propagating) Portevin-Le Chatelier bands can also be effectively investigated by this new technique.

5 Conclusions

1. The strain distribution within individual PLC bands was far from uniform and there existed a wide scattering of the peak band strain (from about 0.4% to 1.5%) and the band width at half height of PLC band strain profiles (from about 0.75 mm to 2.5 mm for test coupons with an initial coupon thickness of 0.95 mm). The effective strain rate inside a PLC band was estimated to be at least 0.1–1 1/s, although the applied nominal strain rates were 1.5×10^{-4} to 5×10^{-5} 1/s.
2. The stress serrations depended on the geometry and size of test coupons and test machine stiffness even when tensile tests were conducted at the same nominal strain rate under displacement control; the time distribution of serrations was related to the PLC bands with various peak strains, band width, and locations (including shoulder sections of test coupons), reflecting the heterogeneity (band nucleation threshold) of the test material.
3. Serrated plastic flow occurred in as-received AA5052-H32 test coupons only after an incubation or critical strain of $\sim$1%; no such threshold strain was observed in any of the thinner or mechanically polished test coupons. It is suggested that the stress-based band nucleation threshold at the mesoscale (over the sheet thickness of the test coupons) is the key to understand spatial and temporal characteristics of both type-C as well as type-B PLC bands in Al-Mg alloys.
4. The high-resolution digital imaging and correlation-based strain mapping was a very effective technique for characterizing the morphology of PLC bands, and the orientation angle of PLC bands was found to be consistent with the macroscopically *localized* deformation band of zero extension in an anisotropic sheet.

Acknowledgment

The authors are grateful to Dr. Tim Focke of NIST for supplying the AA5052-H32 sheet metals used in this investigation and Dr. Frank Mandigo of Olin Metals Research Lab (New Haven, CT) for helping with preparation of standard tensile test coupons and mechanical polishing and chemical etching of test coupons.

References

[1] Cottrell, A. H., 1953, *Dislocations and Plastic Flow in Crystals*. Clarendon Press, Oxford.
[2] Hall, E. O., 1970, *Yield Point Phenomena in Metals and Alloys*. MacMillan, London.
[3] Robinson, J. M., 1994, "Serrated Flow in Aluminum Base Alloys," Int. Mater. Rev., **39**(6), pp. 217–227.
[4] Kubin, L. P., Fressengeas, C., and Ananthakrishna, G., 2002, "Collective Behavior of Dislocations in Plasticity," *Dislocation in Solids*, F. N. N. Nabarro, and J. P. Hirth, eds., Elsevier, New York, Vol. 11, pp. 101–192.
[5] Weinhandl, H., Mitter, F., Bernt, W., Kumar, S., and Pink, E., 1994, "Computer-Assisted Recording of Tensile Tests for the Evaluation of Serrated Flow," Scr. Metall. Mater., **31**(11), pp. 1567–1572.
[6] Pink, E., Bruckbauer, P., and Weinhandl, H., 1998. "Stress-Drop Rates in Serrated Flow of Aluminum Alloys," Scr. Mater., **38**(6), pp. 945–951.
[7] Chihab, K., and Fressengeas, C., 2003, "Time Distribution of Stress Drops, Critical Strain and Crossover in the Dynamics of Jerky Flow." Mater. Sci. Eng., A, **356**, pp. 102–107.
[8] Tong, W., 1997. "Detection of Plastic Deformation Patterns in a Binary Aluminum Alloy," Exp. Mech., **37**(4), pp. 452–459.
[9] Tong, W., 1998, "Strain Characterization of Propagative Deformation Bands," J. Mech. Phys. Solids, **46**(10), pp. 2087–2102.
[10] Smith, B. W., Li, X., and Tong, W., 1998, "Error Assessment for Strain Mapping by Digital Image Correlation," Exp. Tech., **22**(4), pp. 19–21.
[11] Tong, W., and Li, X., 1999, "Evaluation of Two Plastic Strain Mapping Methods," *Proc. of the SEM Annual Conf.*, Cincinnati, pp. 23–26.
[12] Li, X., 2001, "Spatial Characterization and Modeling of Unstable Plastic Flow Patterns in Two Aluminum Alloys," Ph.D. thesis, Yale University, New Haven.
[13] Caron, R. N., and Staley, J. T., 1997, "Effects of Composition, Processing and Structure on Aluminum Alloys," *Materials Selection and Design*, ASM Metals Handbook, Vol. 20, Materials Park, OH, pp. 383–415.
[14] Chihab, K., Estrin, Y., Kubin, L. P., and Vergnol, J., 1987, "The Kinectics of the Portevin-Le Chatelier Bands in an Al-5 at. % Mg Alloy," Scr. Metall. **21**, pp. 203–208.
[15] Schwarz, R. B., and Funk, L. L., 1985, "Kinetics of the Portevin-Le Chatelier Effect in Al6061 Alloy," Acta Metall. **33**, pp. 295–307.
[16] Faciu, C., Molinari, A., Dablij, M., and Zeghloul, A., 1998, "A New Rate-Type Gradient-Dependent Viscoplastic Approach for Stop-and-Go Strain Band Propagation: Numerical vs. Physical Experiments," J. Phys. IV, **8**, pp. Pr8-143–150.
[17] Lebyodkin, M., Dunin-Barkowskii, L., Brechet, Y., Estrin, Y., and Kubin, L. P., 2000, "Spatio-Temporal Dynamics of the Portevin-Le Chatelier Effect: Experiment and Modeling," Acta Mater., **48**, pp. 2529–2541.
[18] Wen, W., and Morris, J. G., 2003, "An Investigation of Serrated Yielding in 5000 Series in Aluminum Alloys Mater. Sci. Eng., A, **354**, pp. 279–285.
[19] Tong, W., Tao, H., Zhang, N., and Hector, L. G., 2005, "Time-Resolved Strain Mapping Measurements of Individual Portevin-Le Chatelier Deformation Bands," Scr. Mater., **53**(1), pp. 87–92.
[20] Hahner, P., Ziegenbein, A., and Neuhauser, H., 2001, "Observation and Modeling of Propagating Portevin-Le Chatelier Deformation Bands in Cu-15 at. % Al polycrystals," Philos. Mag. A, **81**, pp. 1633–1649.
[21] Klose, F. B., Ziegenbein, A., Hagemann, F., Neuhauser, H., Hahner, P., Abbadi, M., and Zeghloul, A., 2004, "Analysis of Portevin-Le Chatelier Serrations of Type B in Al-Mg," Mater. Sci. Eng., A, **369**, pp. 76–81.
[22] Klose, F. B., Weidenmuller, J., Ziegenbein, A., Hahner, P., and Neuhauser, H., 2004, "Plastic Instabilities With Propagation Deformation Bands in Cu-Al alloys," Philos. Mag., **A84**, pp. 467–480.
[23] Rizzi, E., and Hahner, P., 2004, "On the Portevin-Le Chatelier Effect: Theoretical Modeling and Numerical Results," Int. J. Plast., **20**, pp. 121–165.
[24] Ananthakrishna, G., and Bharathi, M. S., 2004, "Dynamical Approach to the Spatiotemporal Aspects of the Portevin-Le Chatelier Effect: Chaos, Turbulence, and Band Propagation," Phys. Rev. E, **70**(2), 026111–1.
[25] Hill, R., 1950, *The Mathematical Theory of Plasticity*, Clarendon Press, Oxford, p. 324.